Electronic Supplementary Material (ESI) for Dalton Transactions.

A novel luminescent Pb(II) - organic framework exhibiting rapid and selective detection of trace amount of NACs and Fe^{3+} with excellent recyclability

Xuan Luo[a], Xiao Zhang*[a,c], Yuanling Duan[a], Xiaolin Wang[b], Jiaming Zhao[b]

Supporting information

Figure cation

Fig. S1 A view of the asymmetric unit and some symmetry-related atoms in **1**

Fig. S2 The IR spectra of H_2L ligand and **1**

Fig. S3 Powder XRD of simulated from the single-crystal data of **1** and synthesized compound **1**

Fig. S4 Thermogravimetric analyses curve of **1**.

Fig. S5 Power patterns of **1** in different temperature.

Fig. S6 Solid-state emission spectra of compound **1** and free H_2L ligand when excited at 260 nm, respectively.

Fig.S7 Emission spectra of compound **1** and free H_2L ligand dispersed in water when excited at 260 nm, respectively.

Fig. S8 Emission spectra of **1** dispersed in different solvents when excited at 260 nm.

Fig. S9 Power patterns of **1** immersed in different solvents at room temperature.

Fig. S10 Solid UV spectra of compound **1.**

Fig. S11 - S18 (a) The luminescence intensity of **1** upon incremental addition of NACs solution (5 mM) in water. (b) Stern-Volmer plot for the luminescence intensity of **1** upon the addition of NACs solution (5 mM) in water.

Fig. S19 - S27 The fitting curve of the luminescence intensity of **1** at different NACs concentration (linear range 0-0.025 mM).

Fig. S28 HOMO and LUMO of H_2L ligand and NACs.

Fig. S29 Spectral overlap between normalized absorbance spectra of NACS and emission spectra of **1**.

Fig. S30 The fitting curve of the luminescence intensity of **1** at different Fe^{3+} concentration (linear range 0-0.13 mM).

Fig. S31 Power XRD patterns of **1** after three recycles.

Fig. S32 Powder XRD patterns of simulated from the single-crystal data of **1** and synthesized compound and Fe^{3+}-1.

Fig. S33 Spectral overlap between normalized absorbance spectra of metal icons and emission spectra of **1**.

Fig. S34 The XPS of Fe^{3+}-1 shows the typical peak of Fe^{3+} at 710 eV.

Fig. S35- S37.The luminescence intensity of 1 upon addition 4 μL and 8 μL of Fe^{3+} ions (25 mM) in drinking, tap, river water.

Table S1 Selected bond lengths (Å) and angles (°) for **1**

Table S2 Summary of quenching constants (K_{SV}) for **1** sensing of NACs at room temperature.

Table S3 Summary of limit detection (M) for **1** sensing of NACs at room temperature.

Table S4 HOMO and LUMO energies for calculated NACs at B3LYP/6-31G* level of theory

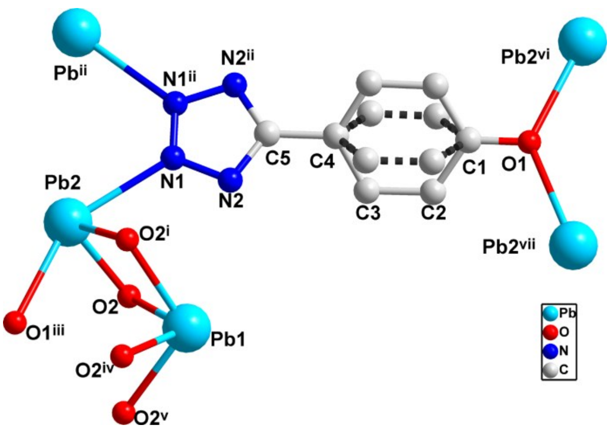

Fig. S1 A view of the asymmetric unit and some symmetry-related atoms in **1**. Symmetry codes: (i) x, y, 1.5-z. (ii) 2-x, y, 1.5-z. (iii) x-0.5, y-0.5, z. (iv) 1-x, 1-y, z-0.5. (v) 1-x, 1-y, 2-z. (vi) 0.5+x, 0.5+y, z. (vii) 1.5-x, 0.5+y, 1.5-z.

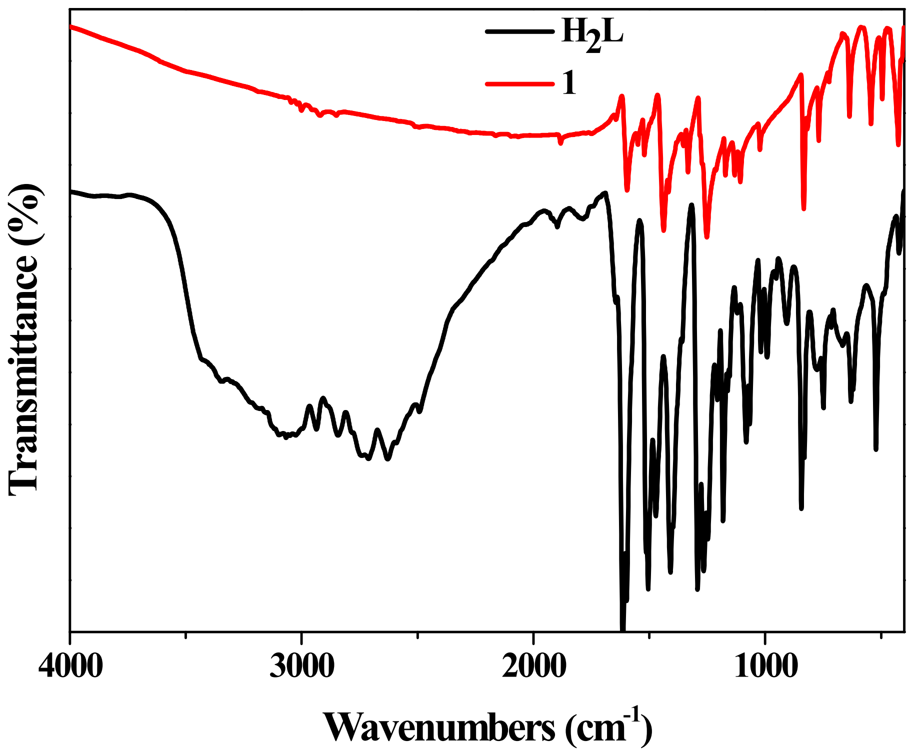

Fig. S2 The IR spectra of H_2L ligand and **1**

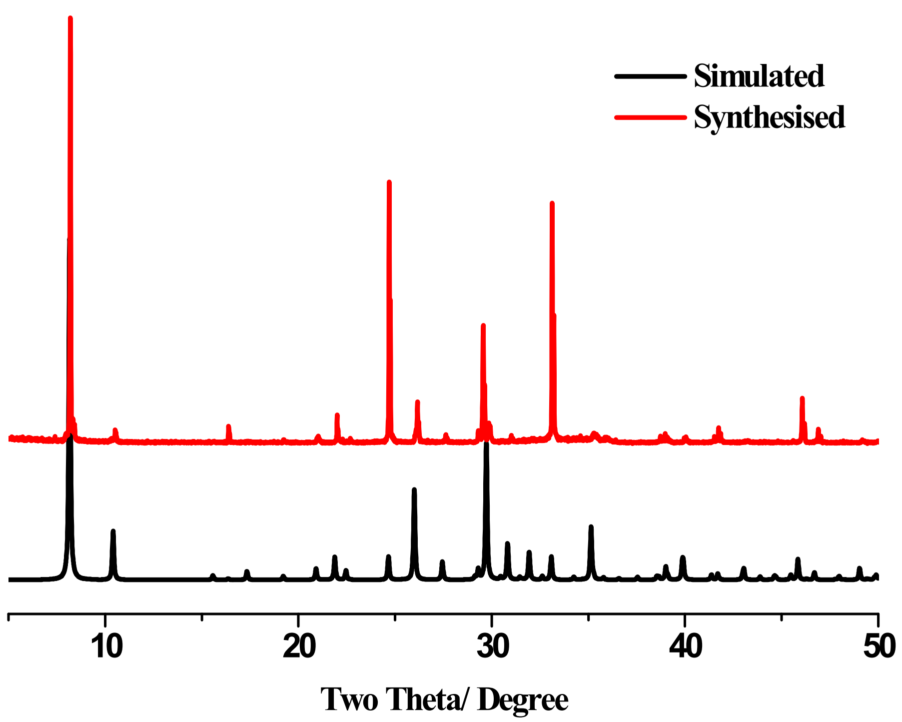

Fig. S3 Powder XRD of simulated from the single-crystal data of **1** (black) and synthesized compound **1.**

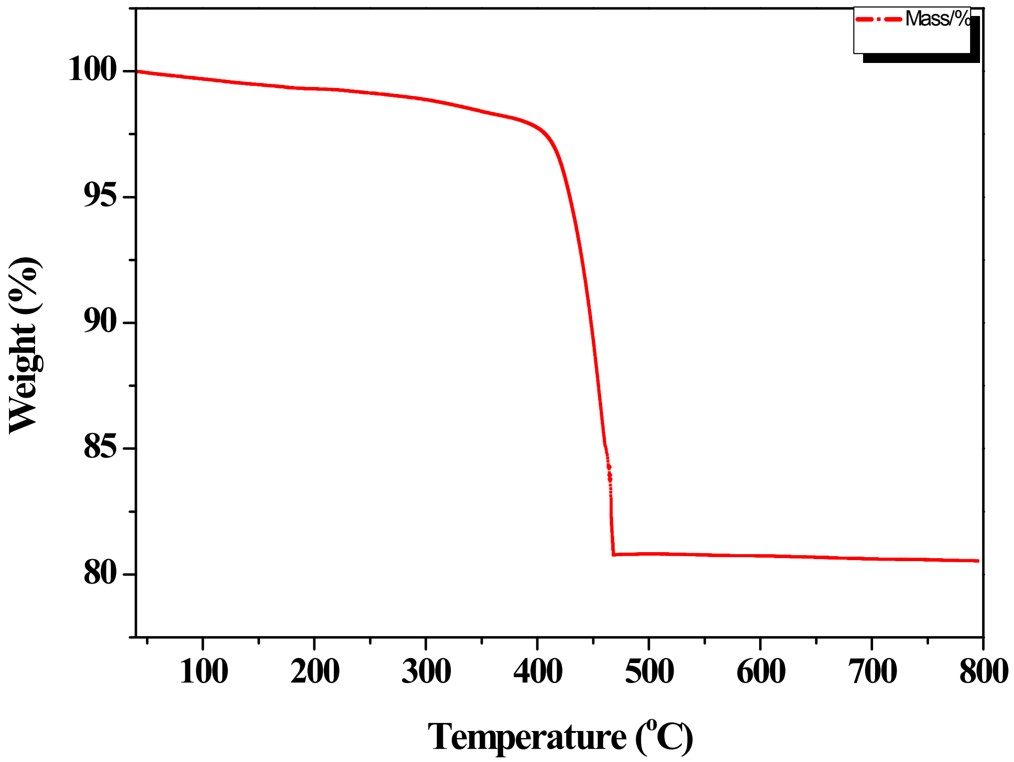

Fig.S4 Thermogravimetric analyses curve of **1**, the weight loss of 80.73 % is close to the calculated value (81.30 %).

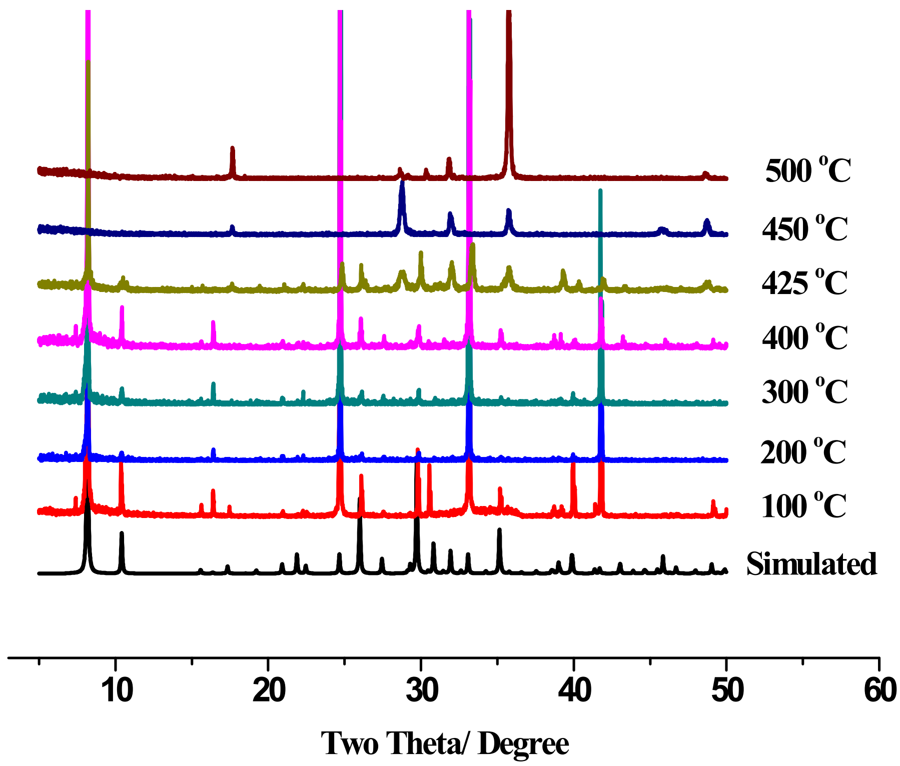

Fig. S5 Power patterns of **1** in different temperature.

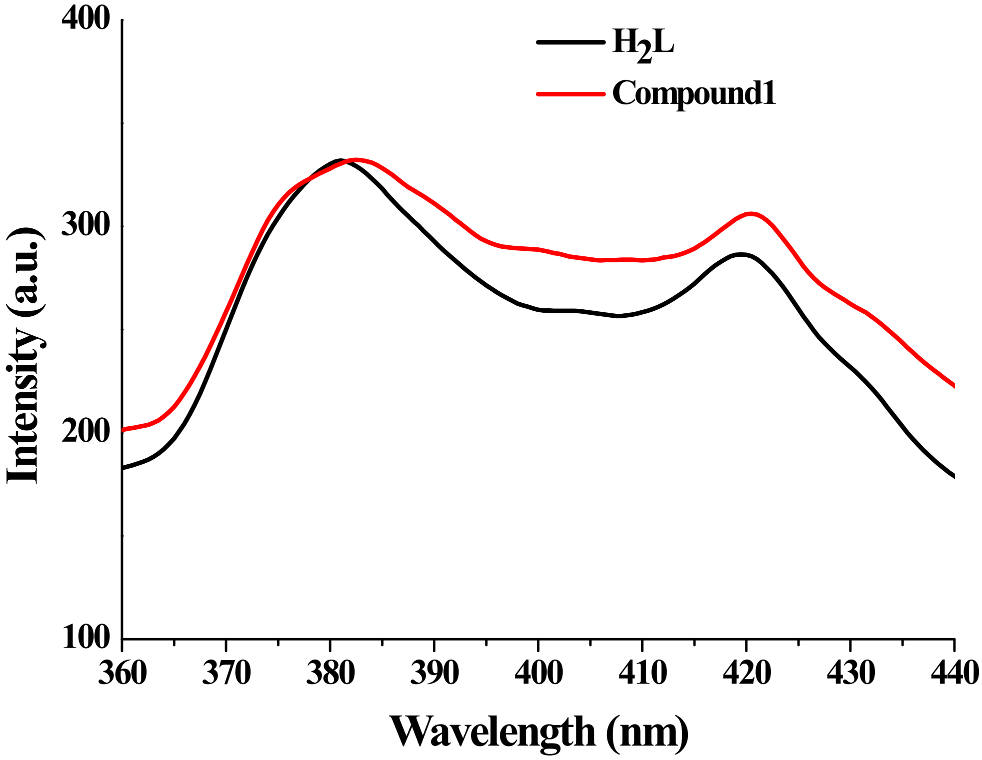

Fig. S6 Solid-state emission spectra of compound **1** and free H_2L ligand when excited at 260 nm, respectively.

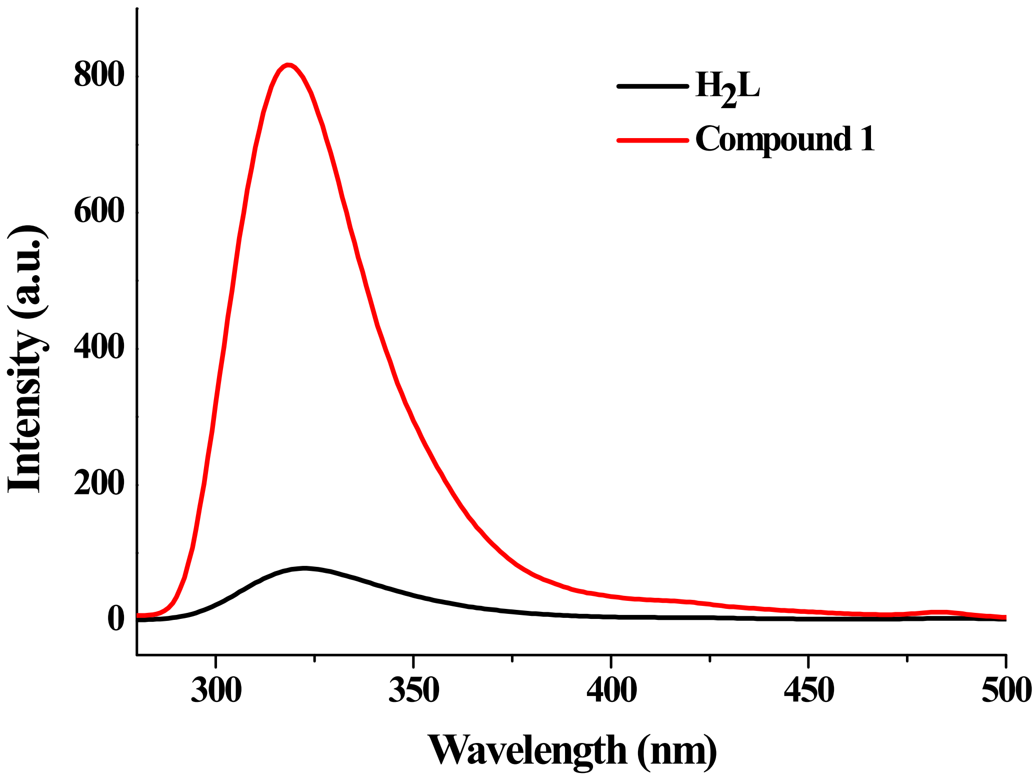

Fig. S7 Emission spectra of compound 1 and free H_2L ligand dispersed in water when excited at 260 nm, respectively.

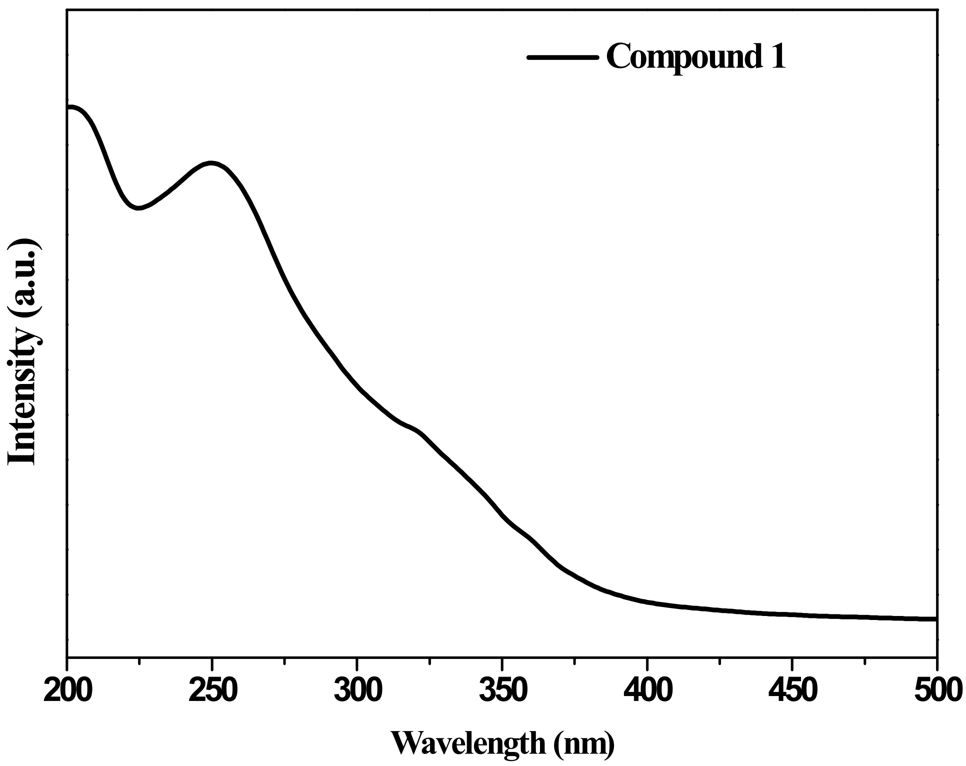

Fig. S8 Solid UV spectra of compound **1.**

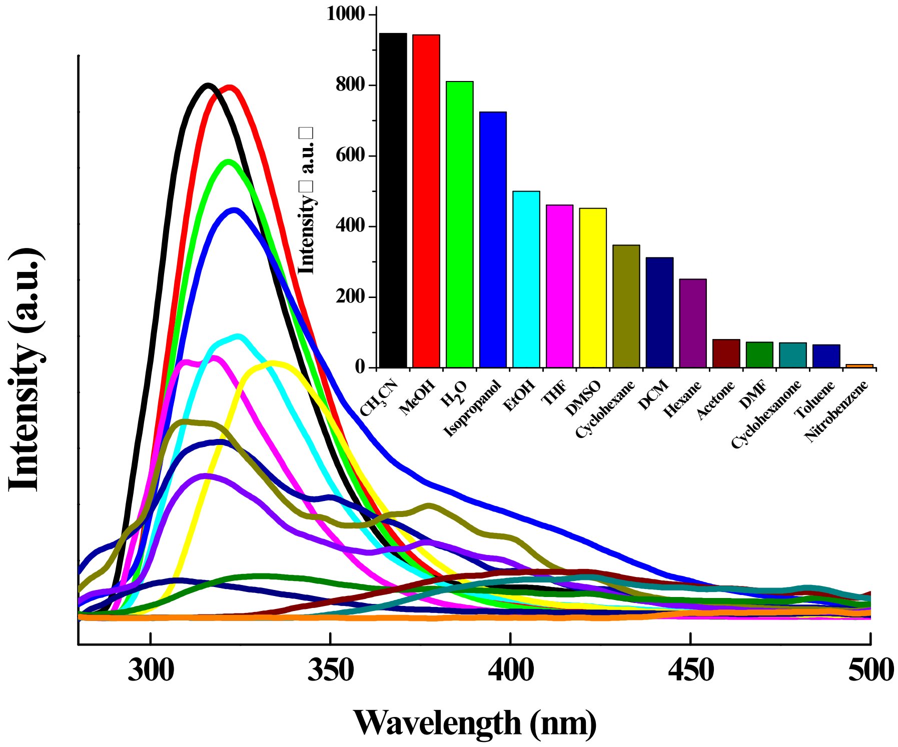

Fig. S9 Emission spectra of **1** dispersed in different solvents when excited at 260 nm.

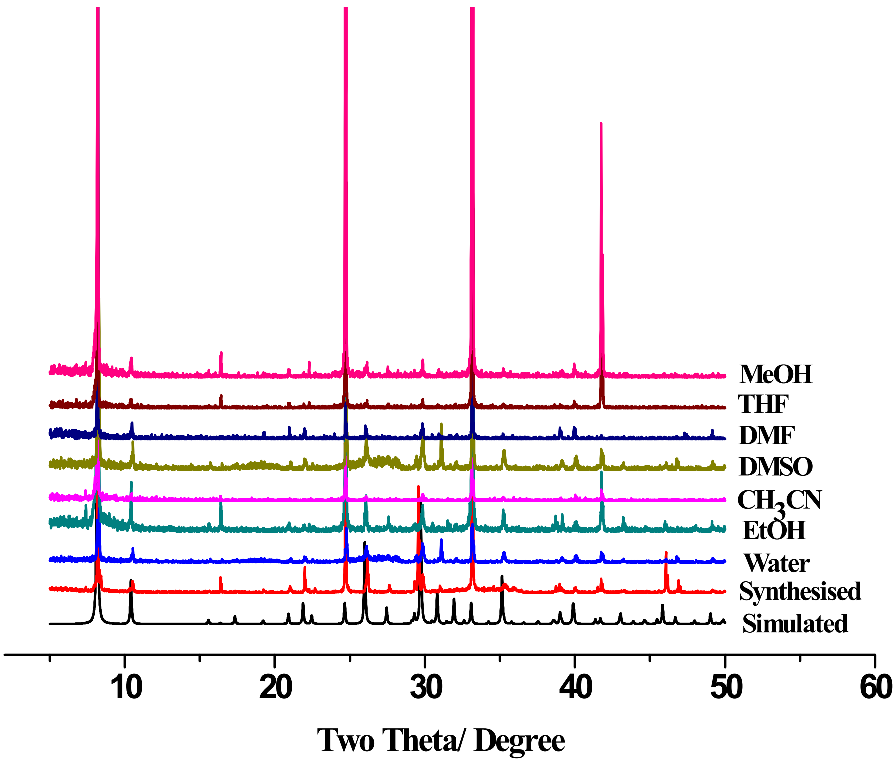

Fig. S10 Power XRD patterns of **1** immersed in different solvents at room temperature.

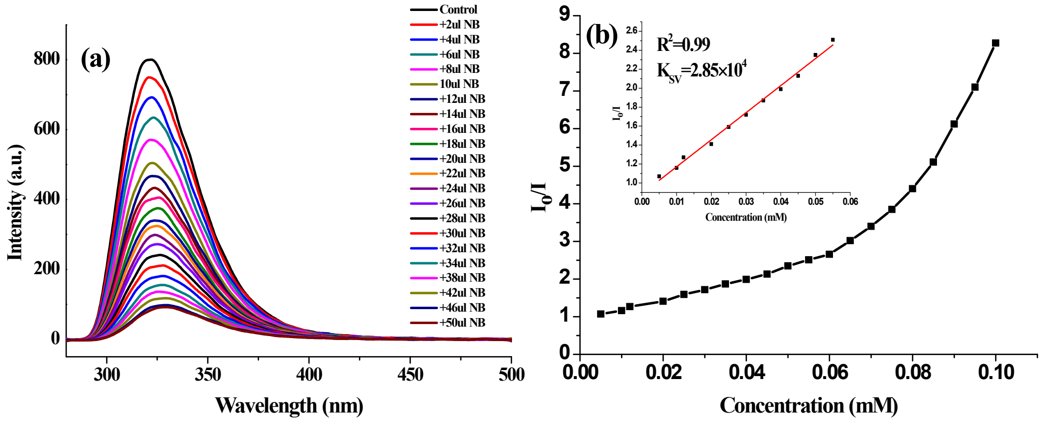

Fig. S11 (a) The luminescence intensity of **1** upon incremental addition of NB solution (5 mM) in water. (b) Stern-Volmer plot for the luminescence intensity of **1** upon the addition of NB solution (5 mM) in water.

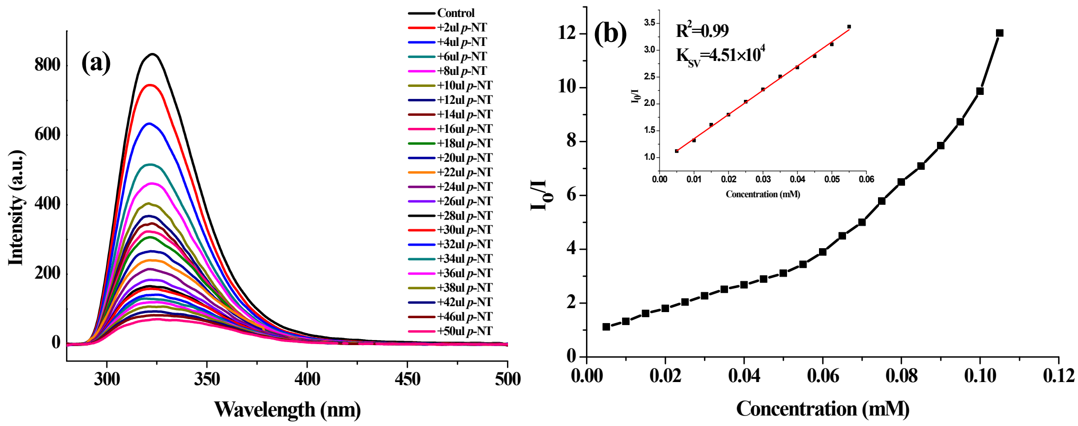

Fig. S12 (a) The luminescence intensity of **1** upon incremental addition of *p*-NT solution (5 mM) in water. (b) Stern-Volmer plot for the luminescence intensity of **1** upon addition of *p*-NT solution (5 mM) in water.

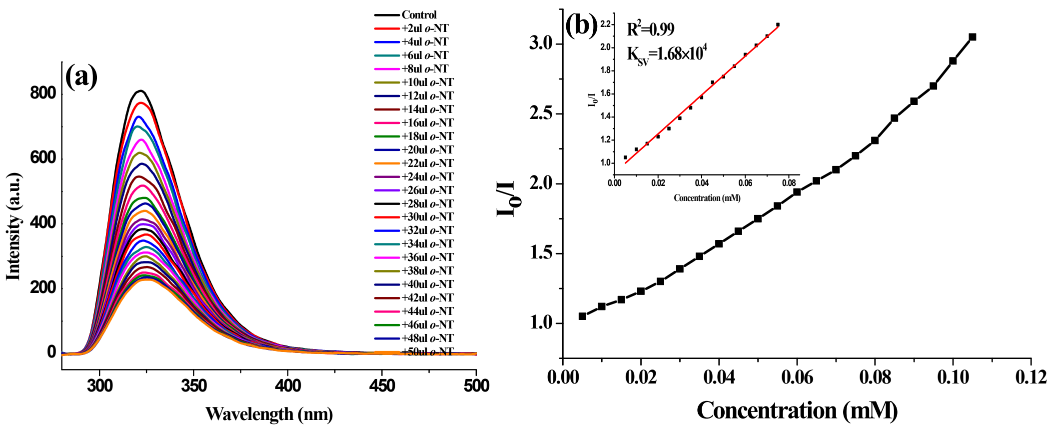

Fig.S13 (a) The luminescence intensity of **1** upon incremental addition of *o*-NT solution (5 mM) in water. (b) Stern-Volmer plot for the luminescence intensity of **1** upon addition of *o*-NT solution (5 mM) in water.

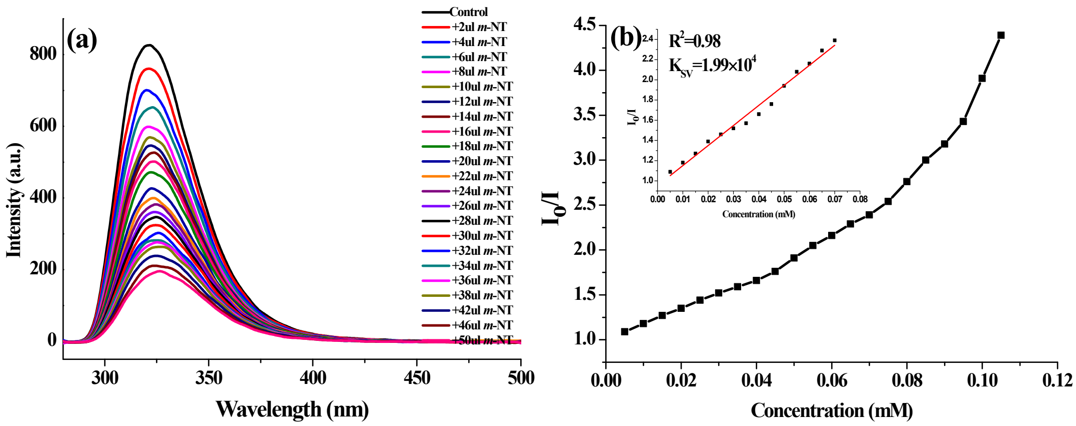

Fig. S14 (a) The luminescence intensity of **1** upon incremental addition of *m*-NT solution (5 mM) in water. (b) Stern-Volmer plot for the luminescence intensity of **1** upon addition of *m*-NT solution (5 mM) in water.

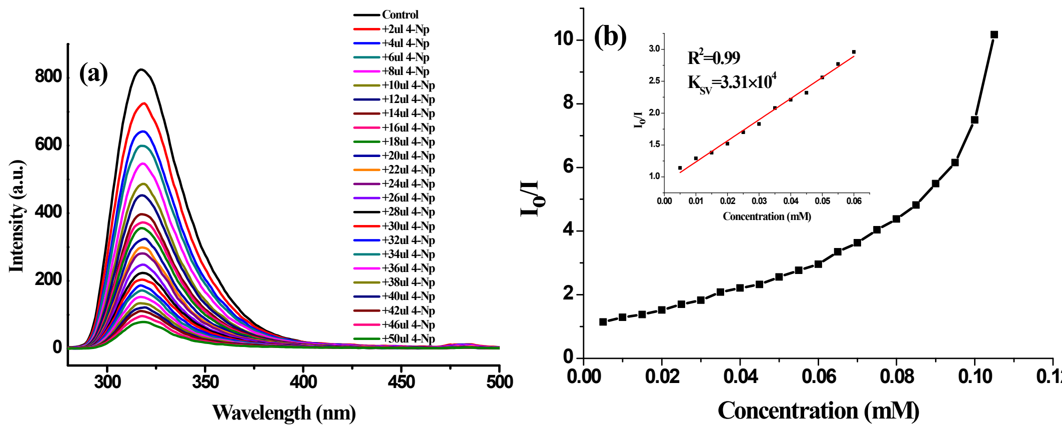

Fig. S15 (a) The luminescence intensity of **1** upon incremental addition of 4-Np solution (5 mM) in water. (b) Stern-Volmer plot for the luminescence intensity of **1** upon addition of 4-Np solution (5 mM) in water.

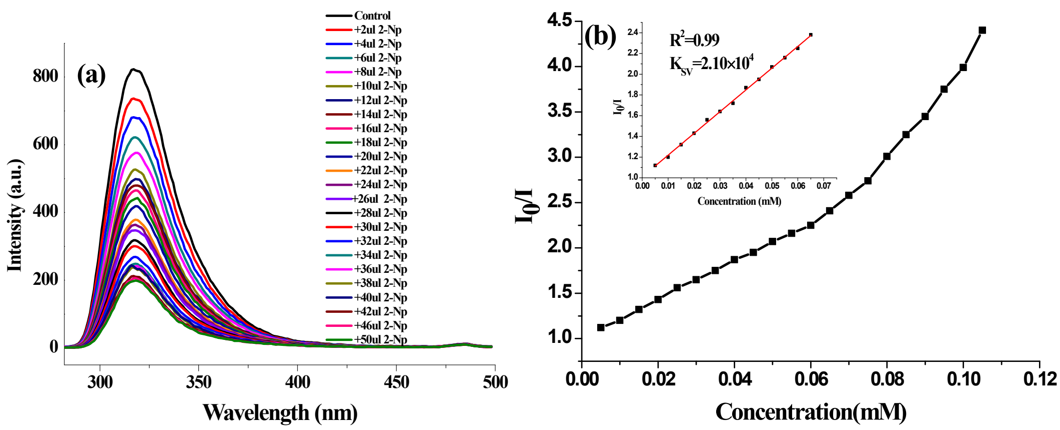

Fig. S16 (a) The luminescence intensity of **1** upon incremental addition of 2-Np solution (5 mM) in water (b) Stern-Volmer plot for the luminescence intensity of **1** upon addition of 2-Np solution (5 mM) in water.

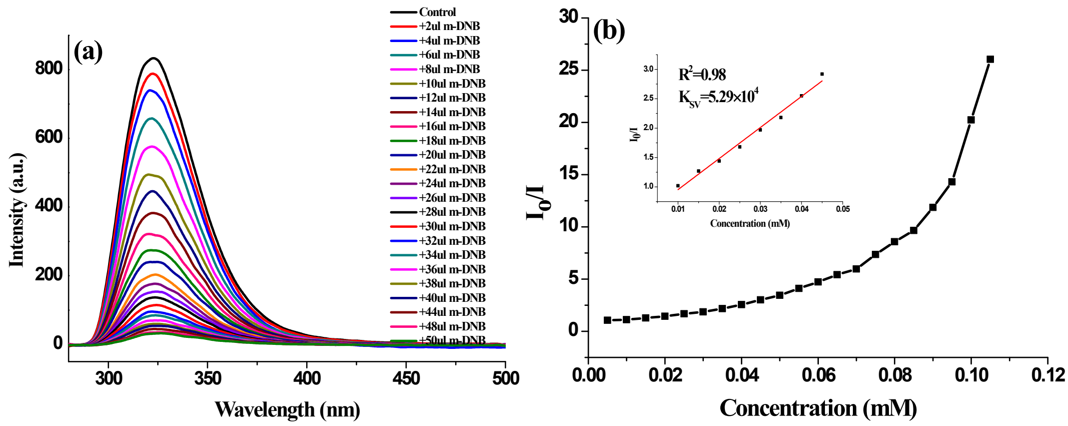

Fig. S17 (a) The luminescence intensity of **1** upon incremental addition of *m*-DNB solution (5 mM in water. (b) Stern-Volmer plot for the luminescence intensity of **1** upon addition of *m*-DNB solution (5 mM) in water.

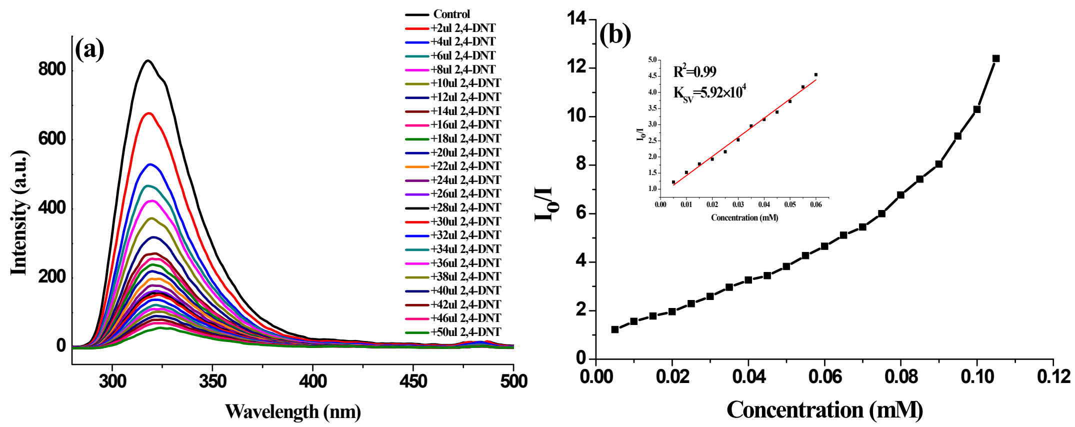

Fig.S18 (a) The luminescence intensity of **1** upon incremental addition of 2, 4-DNT solution (5 mM) in water. (b) Stern-Volmer plot for the luminescence intensity of **1** upon addition of 2, 4-DNT solution (5 mM) in water.

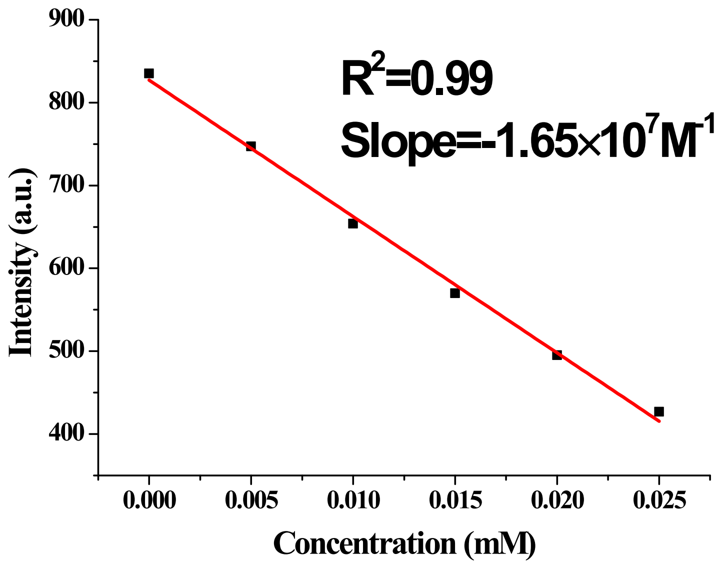

Linear Equation: Y = -16457X + 827.04   R = 0.9960

Slope = 1.65×10^{7} M^{-1}

δ=8.72 (N=10)

Limit detection =3δ/Slope=1.58×10^{-6} M

Fig. S19 The fitting curve of the luminescence intensity of **1** at different PA concentration (linear range 0-0.025 mM).

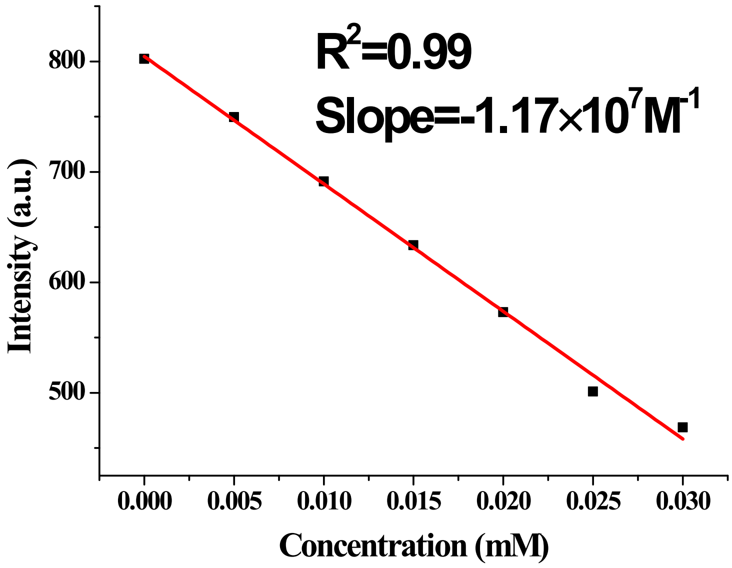

Slope = 1.17×10^{7} M^{-1}

δ=8.72 (N=10)

Limit detection =3δ/Slope=2.24×10^{-6} M

Fig. S20 The fitting curve of the luminescence intensity of **1** at different NB concentration (linear range 0-0.030 mM).

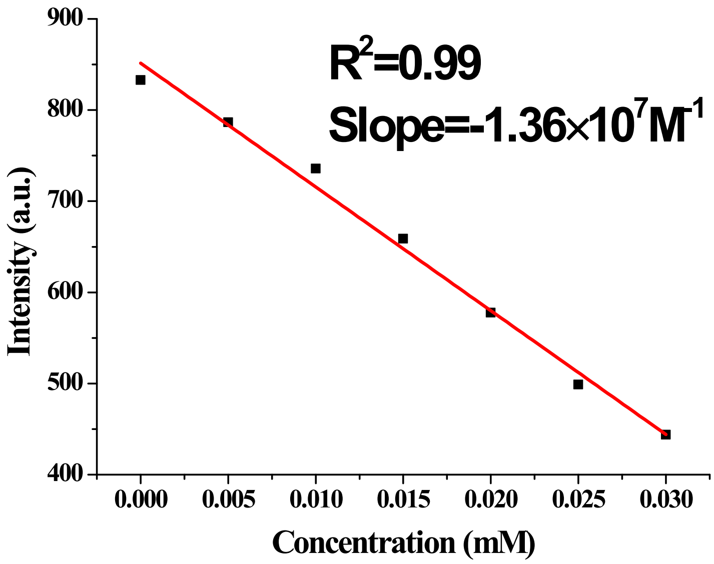

Slope = 1.36×10^{7} M^{-1}

δ=8.72 (N=10)

Limit detection =3δ/Slope=1.92×10^{-6} M

Fig. S21 The fitting curve of the luminescence intensity of **1** at different m-DNB concentration (linear range 0-0.030 mM).

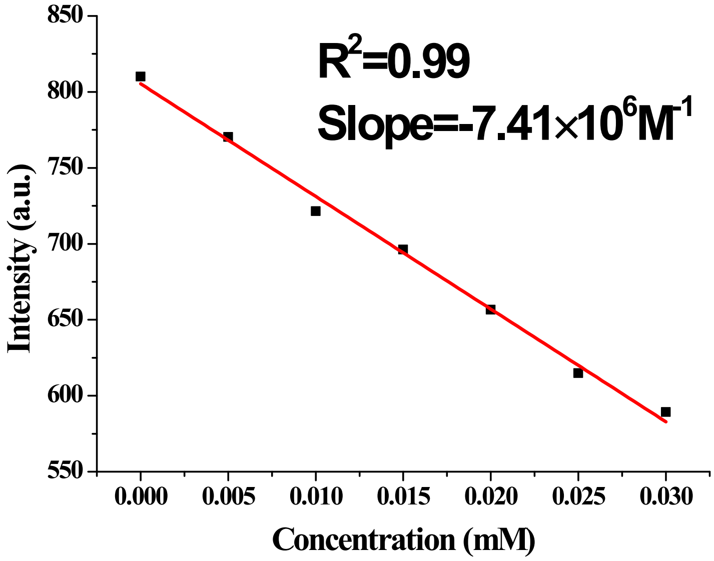

Slope = 7.41× 10^6 M^{-1}

δ=8.72 (N=10)

Limit detection =3δ/Slope=3.53×10^{-6} M

Fig. S22 The fitting curve of the luminescence intensity of **1** at different *o*-NT concentration (linear range 0-0.030 mM).

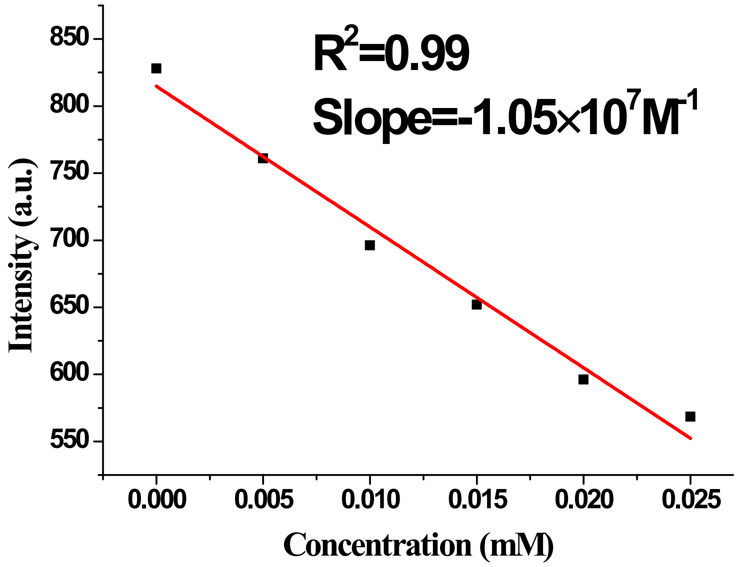

Slope = 1.05× 10^7 M^{-1}

δ=8.72 (N=10)

Limit detection =3δ/Slope=2.49×10^{-6} M

Fig.S23 The fitting curve of the luminescence intensity of **1** at different *m*-NT concentration (linear range 0-0.030 mM).

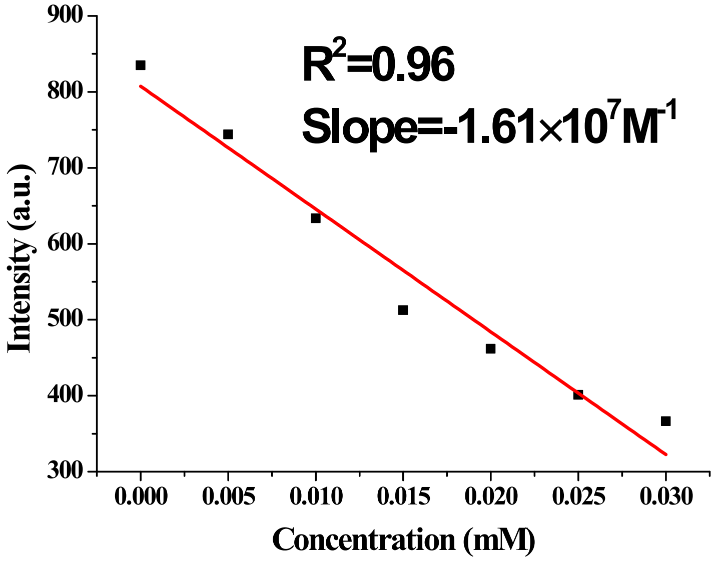

Slope = 1.61× 10^7 M^{-1}

δ=8.72 (N=10)

Limit detection =3δ/Slope=1.62×10^{-6} M

Fig. S24 The fitting curve of the luminescence intensity of **1** at different *p*-NT concentration (linear range 0-0.030 mM).

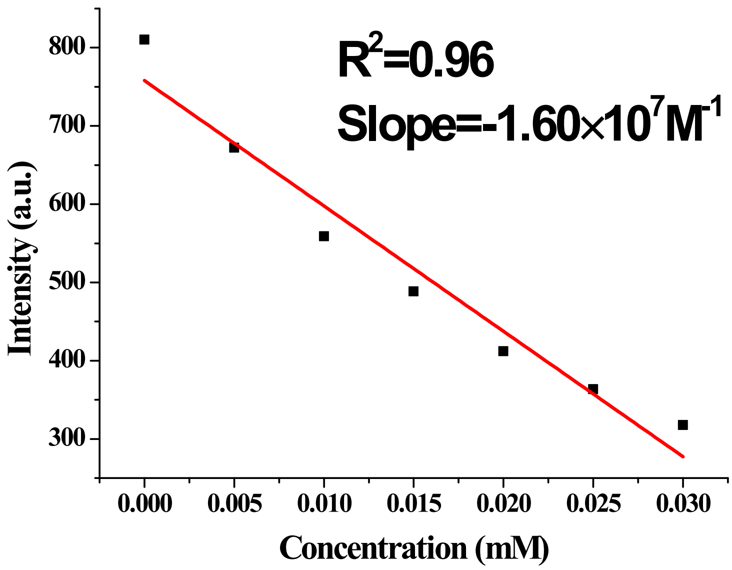

Slope = 1.60× 10^7 M^{-1}

δ=8.72 (N=10)

Limit detection =3δ/Slope=1.63×10^{-6} M

Fig. S25 The fitting curve of the luminescence intensity of **1** at different 2, 4 DNT concentration (linear range 0-0.030 mM).

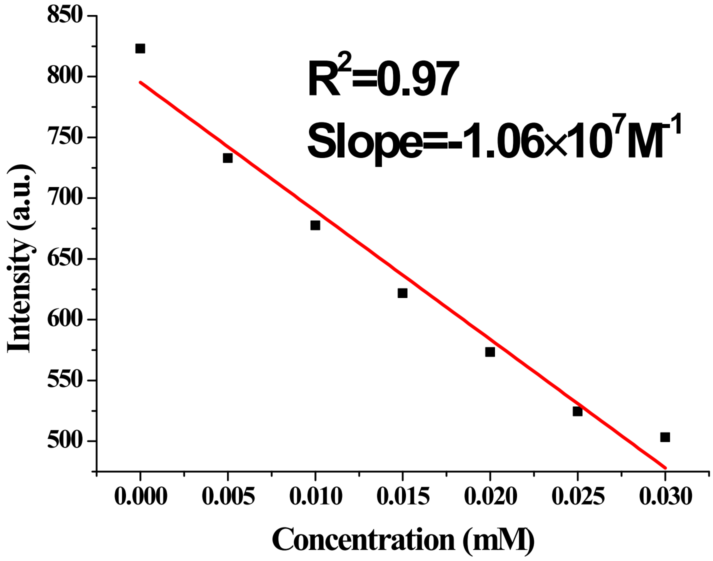

Slope = 1.06× 10^7 M^{-1}

δ=8.72 (N=10)

Limit detection =3δ/Slope=2.46×10^{-6} M

Fig. S26 The fitting curve of the luminescence intensity of **1** at different 2-Np concentration (linear range 0-0.030 mM).

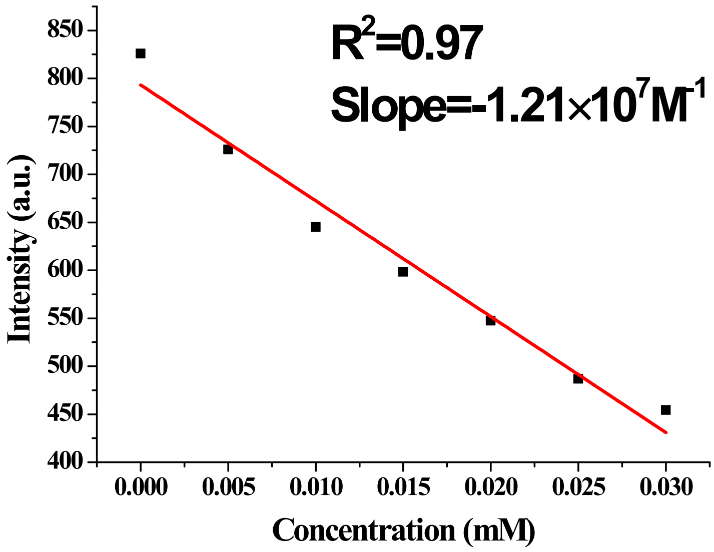

Slope = 1.21× 10^7 M^{-1}

δ =8.72 (N=10)

Limit detection =3δ/Slope=2.16×10^{-6} M

Fig. S27 The fitting curve of the luminescence intensity of **1** at different 4-Np concentration (linear range 0-0.030 mM).

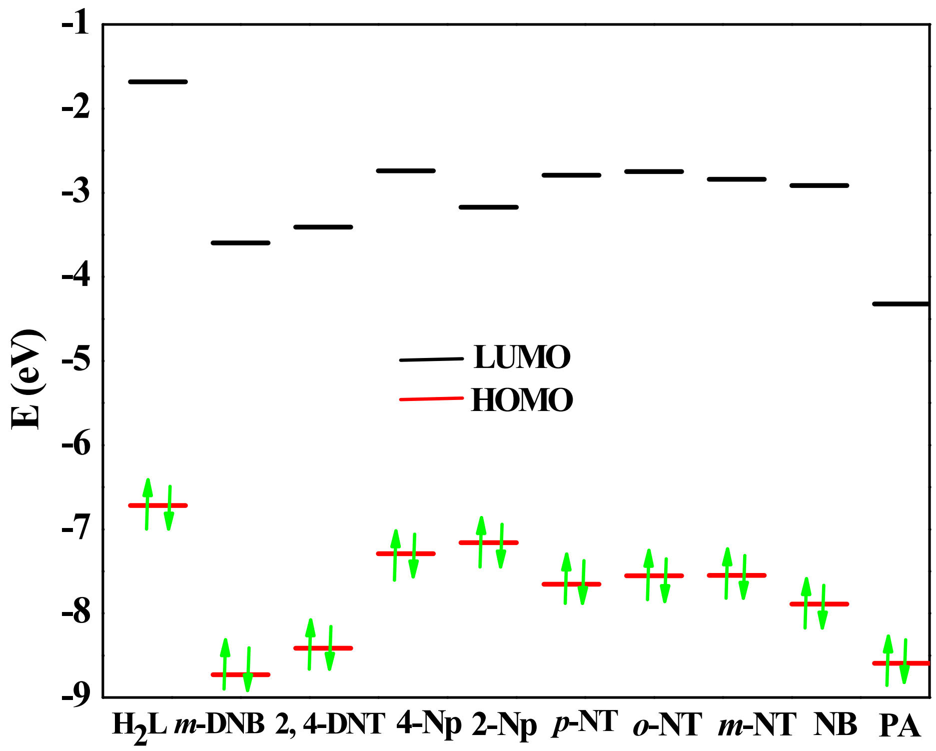

Fig. S28 HOMO and LUMO of H_2L ligand and NACs.

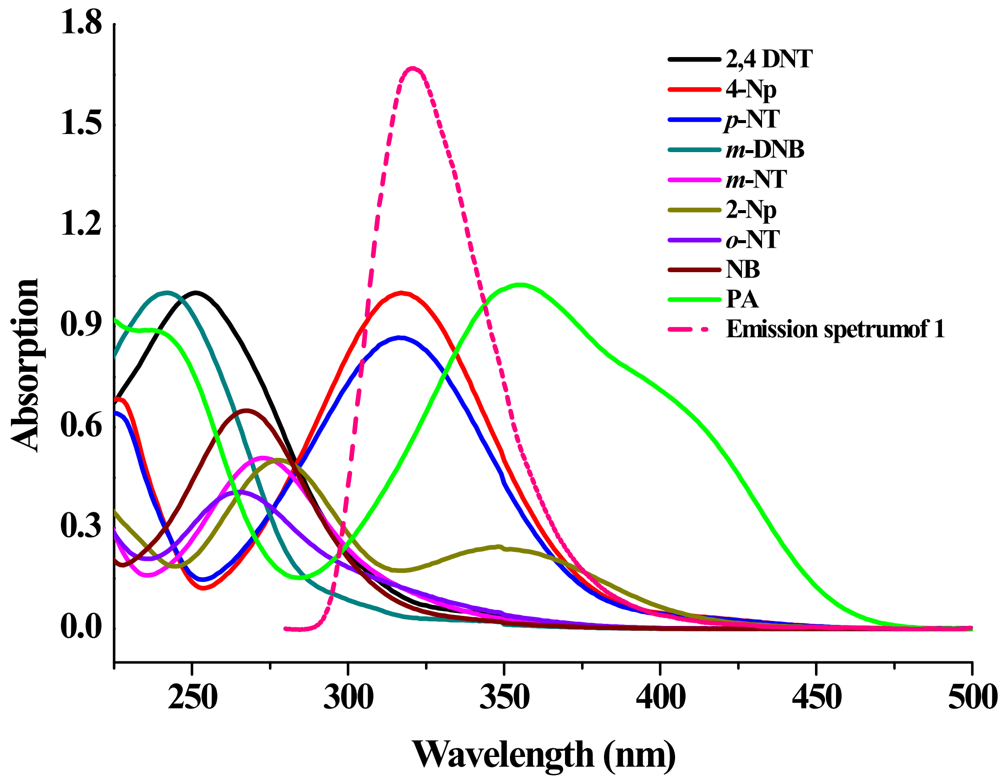

Fig. S29 Spectral overlap between normalized absorbance spectra of NACS and emission spectra of **1**.

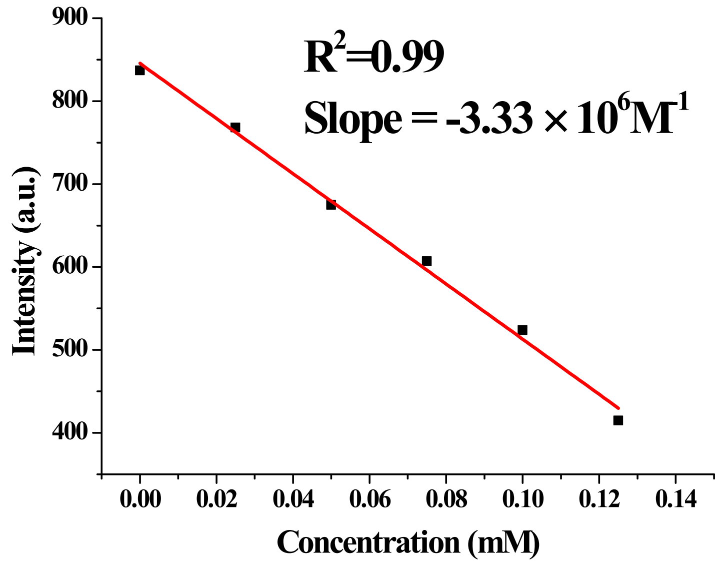

Linear Equation: Y = -3325.7X + 845.52 R = 0.9940

Slope = 3.33 × 10^6 M^{-1}

δ=8.71 (N=10)

Limit detection =3δ/Slope=7.85×10^{-6} M

Fig. S30 The fitting curve of the luminescence intensity of **1** at different Fe^{3+} concentration (linear range 0-0.13 mM).

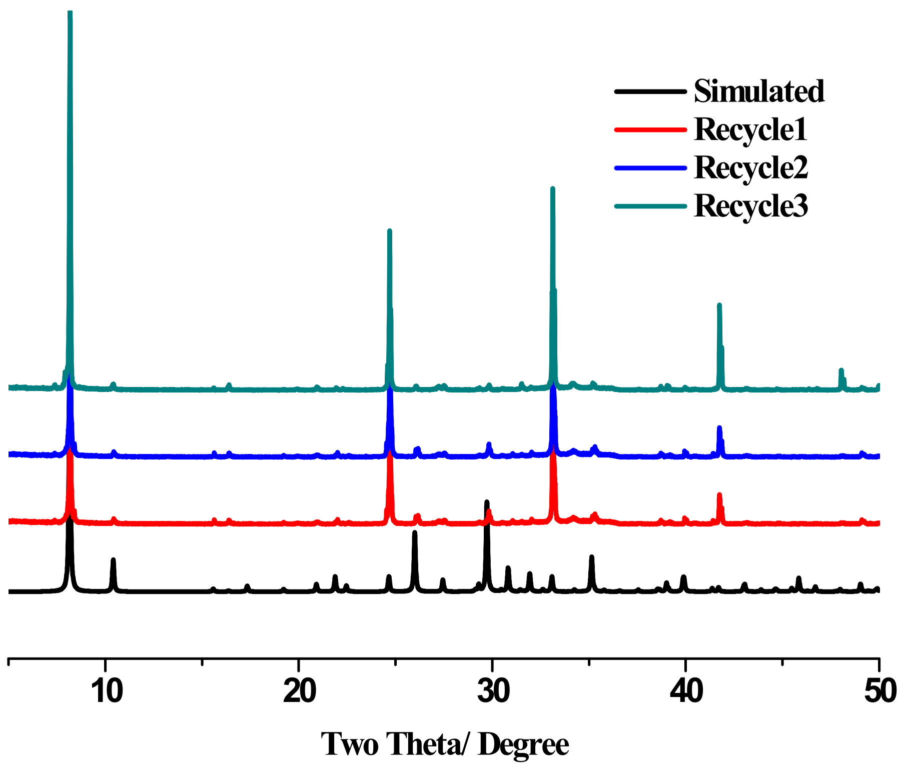

Fig. S31 Power XRD patterns of **1** after three recycles

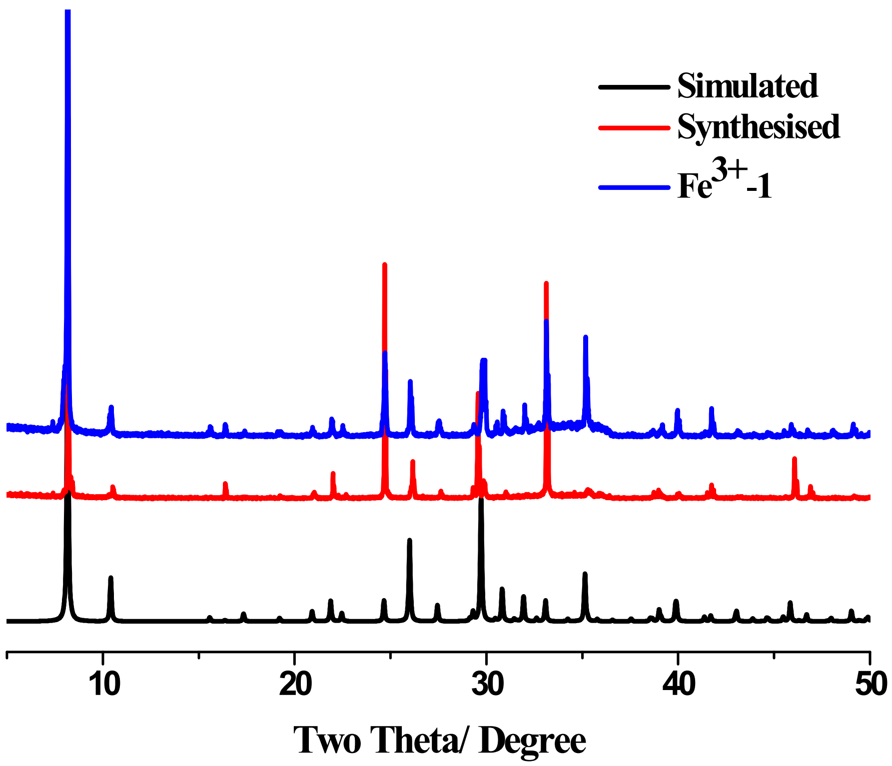

Fig. S32 Powder XRD patterns of simulated from the single-crystal data of **1** and synthesized compound and Fe^{3+}-1

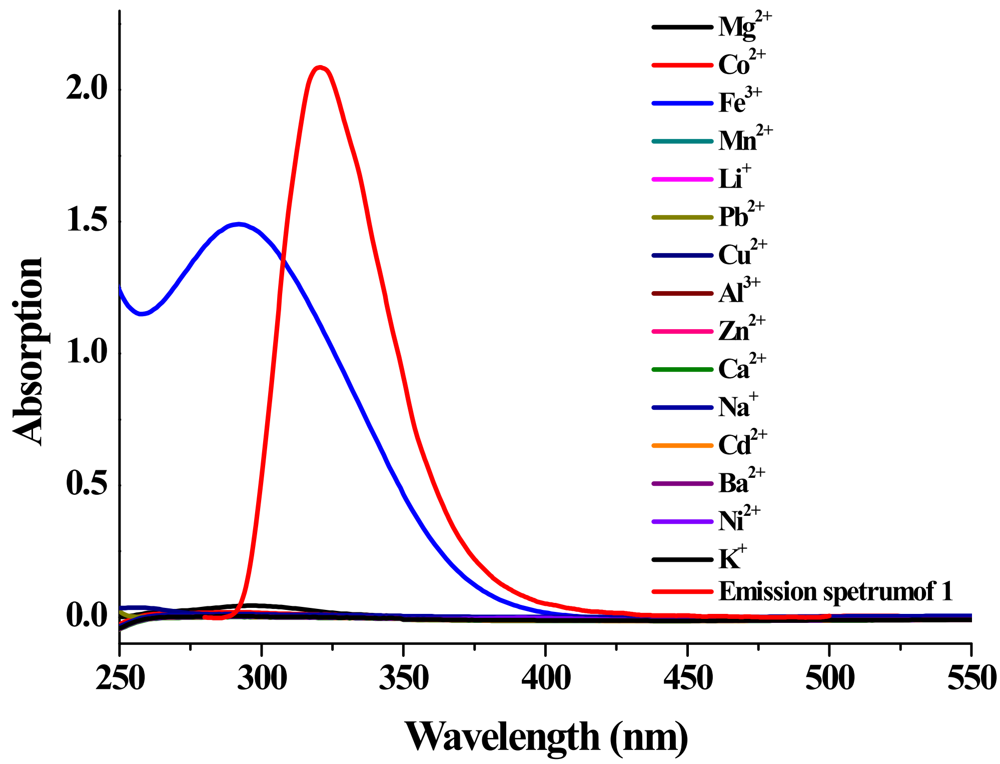

Fig. S33 Spectral overlap between absorbance spectra of metal icons and emission spectra of **1**.

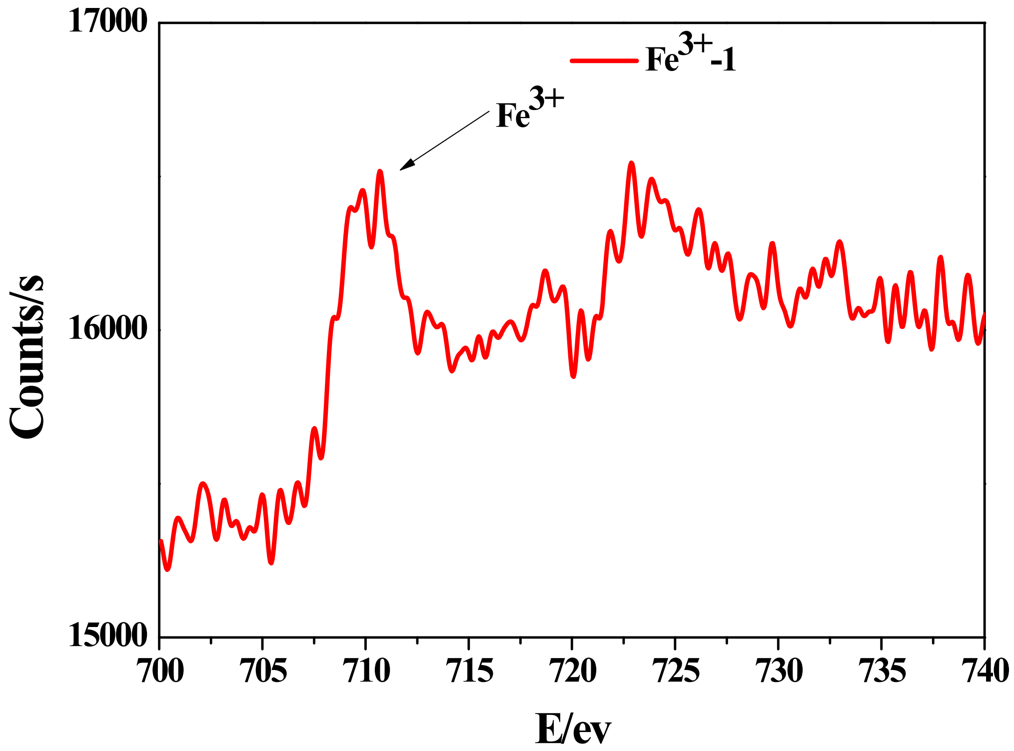

Fig. S34 The XPS of Fe^{3+}-1 shows the typical peak of Fe^{3+} at 710 eV

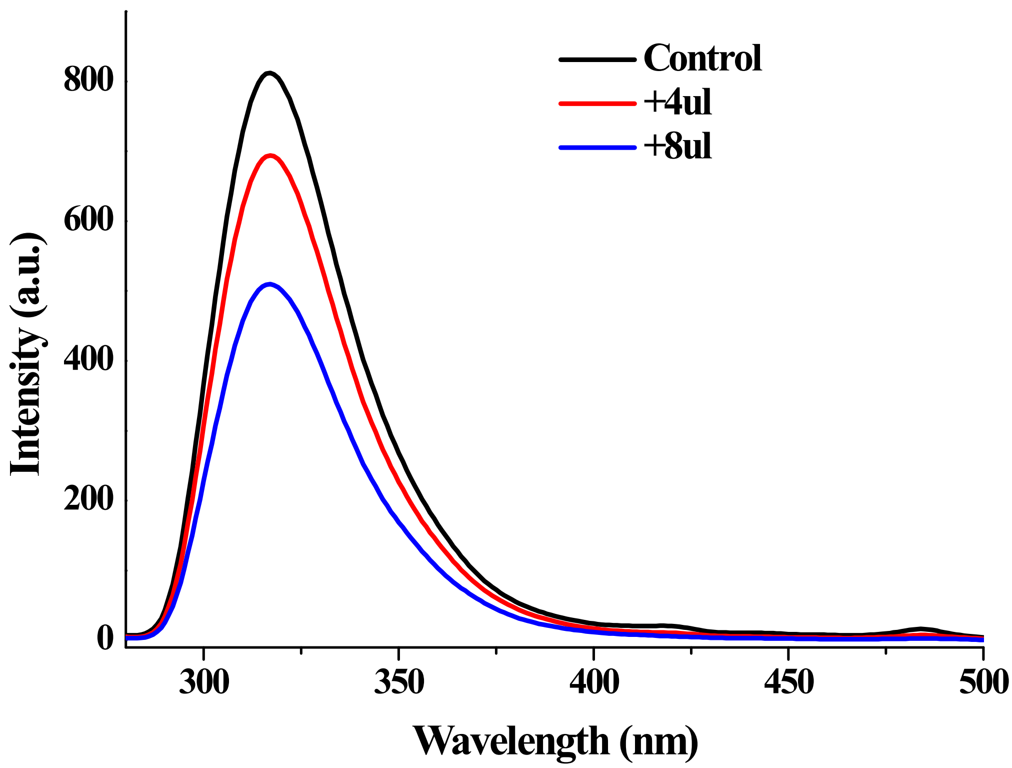

Fig. S35 The luminescence intensity of 1 upon addition 4 μl and 8 μl of Fe^{3+} ions (25 mM) in drinking water.

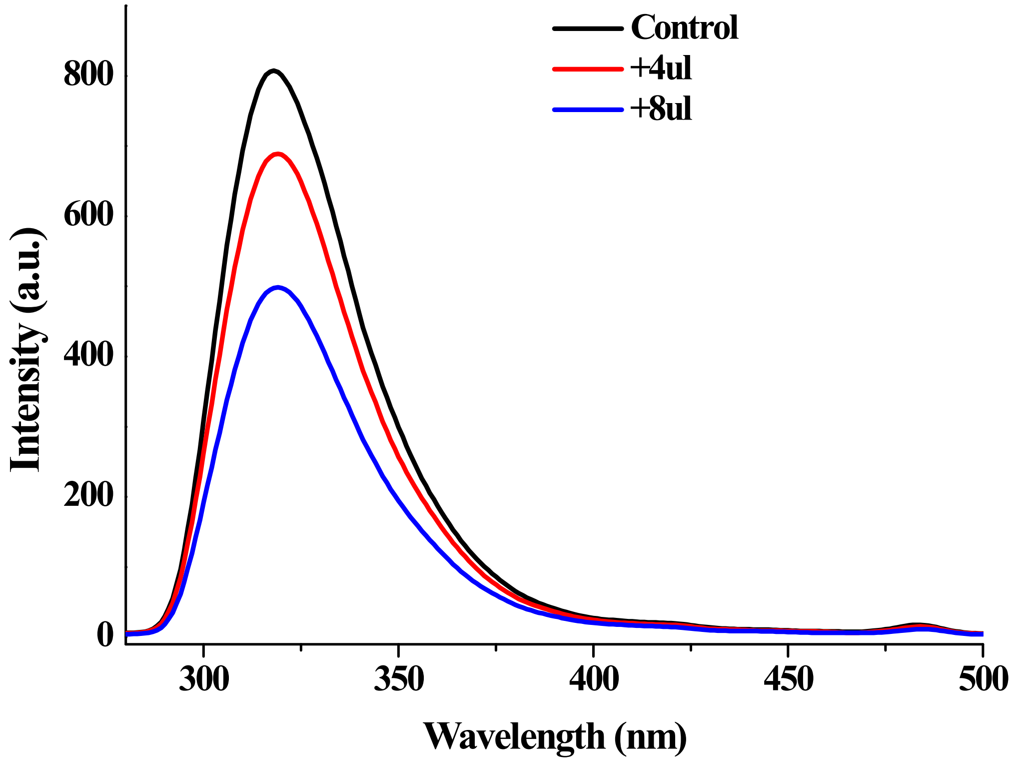

Fig. S36 The luminescence intensity of 1 upon addition 4 µl and 8 µl of Fe^{3+} ions (25 mM) in tap water.

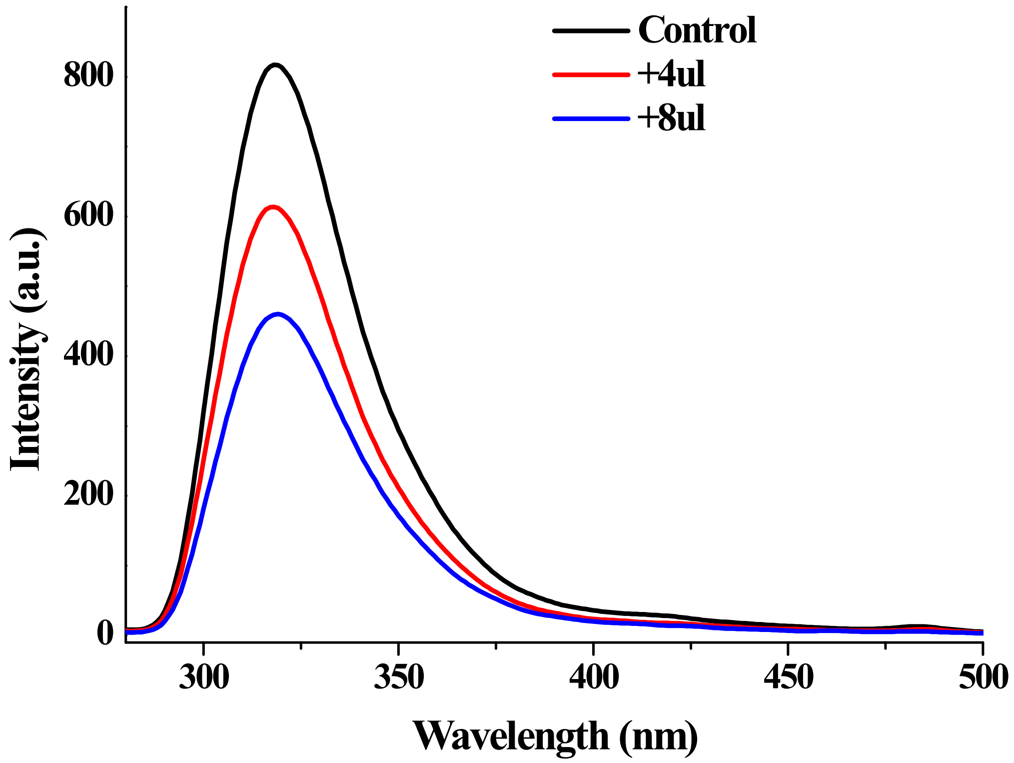

Fig. S37 The luminescence intensity of **1** upon addition 4 µl and 8 µl of Fe^{3+} ions (25 mM) in river water.

Table cation

Table S1 Selected bond lengths (Å) and angles (°) for **1**

Pb1-O2	2.383(3)	Pb2-O1	2.607(4)
Pb2-O2	2.216(3)	Pb2-N1	2.695(11)
$O2^{3}$-Pb1-O2	113.43(10)	$O1^{4}$-Pb2-N1	149.6(3)
$O2^{1}$-Pb1-O2	74.91(12)	O2-Pb2-$O1^{5}$	79.3(2)
$O2^{1}$-Pb1-$O2^{3}$	113.42(10)	O2-Pb2-$O2^{1}$	81.69(11)
$O2^{2}$-Pb1-O2	70.0(2)	O2-Pb2-N1	77.78(17)

Symmetry codes ^{1}+X,+Y,3/2-Z; ^{2}1-X,1-Y,2-Z; ^{3}1-X,1-Y,-1/2+Z; ^{4}-1/2+X,-1/2+Y,+Z;

TableS2 Summary of quenching constants (K_{SV}) for **1** sensing of NACs at room temperature

Analytes	$K_{SV}(M^{-1})$
PA	5.98×10^{4}
2,4-DNT	5.92×10^{4}
m-DNB	5.29×10^{4}
NB	2.85×10^{4}
p-NT	4.51×10^{4}
o-NT	1.68×10^{4}
m-NT	1.99×10^{4}
2-Np	2.10×10^{4}
4-Np	3.31×10^{4}

TableS3 Summary of Limit detection (M) for **1** sensing of NACs at room temperature

Nitro explosives	Slope(M^{-1})	Limit detection(M)
PA	1.65×10^{7}	1.58×10^{-6}
NB	1.17×10^{7}	2.24×10^{-6}
m-DNB	1.36×10^{7}	1.92×10^{-6}
o-NT	7.41×10^{6}	3.53×10^{-6}
m-NT	1.05×10^{7}	2.49×10^{-6}

p-NT	1.61×10^{7}	1.62×10^{-6}
2,4-DNT	1.60×10^{7}	1.63×10^{-6}
2-Np	1.06×10^{7}	2.46×10^{-6}
4-Np	1.21×10^{7}	2.16×10^{-6}

Molecular Orbital Calculations

The electronic properties of L ligand and NACs were studied utilizing the density functional theory (DFT) compountation. Gaussian 09 suite of programs and a hybrid functional, B3LYP were employed. [1-4]

TableS4 HOMO and LUMO energies for calculated NACs and H_2L at B3LYP/6-31G* level of theory[1]

Analytes	Homo(ev)	LUmo(ev)	Bond gap
PA	-8.595166	-4.320934	4.274232
2,4-DNT	-8.41361	-3.409107	5.004502
p-NT	-7.655022	-2.792225	4.862798
NB	-7.887787	-2.912631	4.975156
m-DNB	-8.730522	-3.596104	5.134419
o-NT	-7.554773	-2.746777	4.807996
m-NT	-7.55031	-2.838932	4.711378
2-Np	-7.160373	-3.172671	3.987702
4-Np	-7.290064	-2.73967	4.550394
H_2L	-6.717239	-1.682964	5.034275

[1] M. J. Frisch, G. W. Trucks, H. B. Schlegel, G. E. Scuseria, M. A. Robb, J. R. Cheeseman, G. Scalmani, V. Barone, B. Mennucci, G. A. Petersson, H. Nakatsuji, M. Caricato, X. Li, H. P. Hratchian, A. F. Izmaylov, J. Bloino, G. Zheng, J. L. Sonnenberg, M. Hada, M. Ehara, K. Toyota, R. Fukuda, J. Hasegawa, M. Ishida, T. Nakajima, Y. Honda, O. Kitao, H. Nakai, T. Vreven, J. J. A. Montgomery, J. E. Peralta, F. Ogliaro, M. Bearpark, J. J. Heyd, E. Brothers, K. N. Kudin, V. N. Staroverov, T. Keith, R. Kobayashi, J. Normand, K. Raghavachari, A. Rendell, J. C. Burant, S. S. Iyengar, J. Tomasi, M. Cossi, N. Rega, J. M. Millam, M. Klene, J. E. Knox, J. B. Cross, V. Bakken, C. Adamo, J. Jaramillo, R. Gomperts, R. E. Stratmann, O. Yazyev, A. J. Austin, R. Cammi, C. Pomelli, J. W. Ochterski, R. L. Martin, K. Morokuma, V. G. Zakrzewski, G. A. Voth, P. Salvador, J. J. Dannenberg, S. Dapprich, A. D. Daniels, O. Farkas, J. B. Foresman, J. V. Ortiz,

J. Cioslowski and D. J. Fox, Gaussian 09, Revision C.01, Gaussian, Inc., Wallingford CT, **2010**.
[2]A. D. Becke, *Physical Review A*, **1988**, *38*, 3098-3100.
[3]C. Lee, W. Yang and R. G. Parr, *Physical Review B*, **1988**, *37*, 785-789
[4]A. D. Becke, *J. Chem. Phys.*, **1993**, *98*, 5648-5652